Dalton Transactions

Accepted Manuscript

ROYAL SOCIETY OF CHEMISTRY

www.rsc.org/dalton

Journal Name

RSCPublishing

ARTICLE

Cite this: DOI: 10.1039/x0xx00000x

Received 00th January 2012,
Accepted 00th January 2012

DOI: 10.1039/x0xx00000x

www.rsc.org/

Tin (II) ketoacidoximates: synthesis, X-ray structures and processing to tin (II) oxide

Jayaprakash Khanderi,[a] Bambar Davaasuren,[a] Buthainah Ameen Alshankiti [a] and Alexander Rothenberger [a]*

Tin (II) ketoacidoximates of the type $[HON{=}CRCOO]_2Sn$ (R = Me **1**, CH_2Ph **2**) and $(MeON{=}CMeCOO)_3Sn]^-NH_4^+\cdot 2H_2O$ **3** were synthesized by reacting pyruvate- and hydroxyl- or methoxylamine $RONH_2$ (R = H, Me) with tin (II) chloride dihydrate $SnCl_2\cdot 2H_2O$. The single crystal X-ray structure reveals the geometry at Sn atom as trigonal bipyramidal in **1**, **2** and trigonal pyramidal in **3**. Inter- or intramolecular hydrogen bonding is observed in **1-3**. Thermogravimetric (TG) analysis shows the decomposition of **1-3** to SnO occurs at ca. 160°C. The evolved gas analysis during TG indicates complete loss of the oximato ligand in one step for **1** whereas a small organic residue is additionally removed at temperature >400°C for **2**. Above 140°C $[HON{=}C(Me)COO]_2Sn$ (**1**) decomposes in air to spherical SnO particles of size 10-500 nm. Spin coating of **1** on Si or glass substrate followed by heating at 200°C results in uniform film of SnO. The band gap of the produced SnO film and nanomaterial was determined by diffuse reflectance spectroscopy and found to be in the range of 3.0-3.3 eV. X-ray photoelectron spectroscopy indicates surface oxidation of the SnO film to SnO_2 in ambient atmosphere.

Introduction

Semiconducting stannic oxide (SnO_2) and stannous oxide (SnO) have attracted considerable research interest in the area of electronics and optoelectronics. SnO_2 finds application in transparent conducting electrodes as indium tin oxide (ITO),[1, 2] thin film transistors,[3, 4] sensors,[5, 6] heat reflecting filters[7] and solar cells.[7] The research on SnO is focused on the synthesis of nanostructures[8-12] as anode material in rechargeable Li ion battery.[13, 14] Tin (II) oxide is also a versatile intermediate to metallic tin,[15] Sn_3O_4[16, 17] and SnO_2.[18] The SnO thin films have shown a hole mobility of 2.4 $cm^2V^{-1}s^{-1}$, largest amongst the *p*-type oxide semiconductors.[19] Antimony doped SnO shows *n*-type conduction[20] opening the possibility of ambipolar oxide TFTs.[21] Homo-junction *p-n* diode with *p*-type SnO and *n*-type SnO_2[22] thin film transistors and inverters have been investigated.[19, 23-27] The recent literature reports a variety of physical methods such as e-beam evaporation, reactive/radio-frequency/magnetron sputtering and pulsed laser deposition to deposit *p*-type SnO thin films.[28-30] Chemical methods involve vapor phase deposition using molecular precursors such as $Sn_6O_4(OSiMe_3)_4$, $[\{Sn(OSiMe_3)_2\}_2]$,[31] Sn(II)*bis*(ureide) (ureide = $^tBuNCONMe_2$),[32] *bis*(1-dimethylamino-2-methyl-2propoxy)tin[33] $[Sn(\mu\text{-}ONep)_2]_\infty$ (ONep = OCH_2CMe_3)[34] and solution based methods using $SnCl_2\cdot 2H_2O$ and $NH_{3(aq.)}$.[35] The formation of elemental tin in SnO films[31,34] and sub-stoichiometric tin oxide[34] at higher deposition temperatures (>300°C) are the drawbacks of reported routes.[31, 34, 35] The challenges in the preparation of SnO films are to find a low-temperature route to crystalline SnO, avoiding disproportionation or oxidation to SnO_2 and the scale-up of optimized SnO film deposition.[19, 22,32,36,37]

Metal complexes with oxime/oximate ligands have been extensively studied and reviewed.[38, 39] One important aspect of oximate ligands, derived from the reaction of pyruvic or glyoxylic acid with hydroxylamines, are the complete decomposition to H_2O, CO_2, CH_3CN and functionalized nitriles below 200°C.[40, 41] Thus, it is of interest to examine oximate complexes of tin (II) that could address the challenges associated with SnO formation at lower temperatures.

Cyanoximate and ketoacidoximate complexes of Sn(IV) have been reported.[42,43] The Sn(IV) in cyanoximate complexes, which also show cytotoxicity, are mononuclear and tetranuclear with trigonal pyramidal geometry,[42] whereas Sn(IV) ketoacidoximates are reported to be monomeric with Sn(IV) in octahedral and trigonal bipyramidal geometry.[43] The other reported complexes contain ketoacidoximate ligands with Pd, Ru, Rh, Ir,[44, 45] Mn,[46] Ti,[47] Ni,[48] Cu,[49, 50] Co,[44, 51, 52] Zn,[53] Cd,[50] alkali,[54] and alkaline earth[55] metal ions. The interest in these complexes were due to the fact that: 1) they act as intermediate in the metal activated synthesis of α-amino acids,[45] 2) the oximate ligands are structurally analogous to 2-amino acids and the complexes have shown medical and biological functions[46, 52, 56] and 3) they are used in the synthesis of metal [57] and metal oxide[57-61] nanoparticles and thin films.[53, 61]

Here, we report the synthesis, crystal structures of tin (II) ketoacidoximate complexes **1-3**, experimental condition for the synthesis and detailed characterization of SnO nanoparticles and thin films that were obtained by the decomposition of **1** and **2**.

Result and discussion

The tin (II) ketoacidoximate complexes **1-3** were synthesized by the condensation reaction of *α*-ketocarboxylate and hydroxyl- or methoxyl amine with tin (II) chloride dihydrate in water (Scheme 1). **1** and **2** are isolated as crystalline solids with good yield (67-78 %) whereas **3** was isolated in poor yield (~10 %). All the complexes are soluble in N,N-dimethyl formamide and dimethyl sulfoxide and sparingly soluble in methanol and ethanol. The IR spectra of **1-3** shows characteristic absorptions between 1650-550 cm^{-1} (ESI Fig. S1). The absorption bands at 1620 cm^{-1} (C=N), 1590 cm^{-1} (asymmetric vibrations of COO^-),[51] 1350 cm^{-1} (-C=O symmetric or CH_3) , 1050 cm^{-1} (N-O), 850 cm^{-1} (-OCO- in plane)[43] could be assigned unambiguously. The appearance of ν(sym) and ν(asym) COO band indicate possible π-delocalization of C–O bond. The absorption bands at 3280-3290 cm^{-1} for **3** could be assigned to NH stretching vibrations of the ammonium ion. The NMR chemical shifts observed for **1**, **2** and **3** are in agreement with the previously reported transition metal complexes.[51, 53]

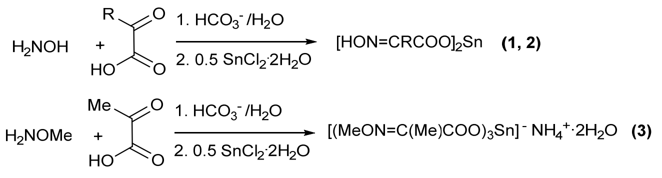

Scheme 1. Synthesis of Sn (II) ketoacidoximates, where R = Me **1**, CH_2Ph **2**.

Description of molecular structures of 1-3

The crystal structure of **1**, **2** and **3** are determined from single crystal X-ray diffraction data. Fig. 1a-c shows the molecular geometry, bonding and atom labelling of **1**, **2** and **3**. The details on data collection and refinement are summarized in Table 1.

The crystal structure of **1** and **2** contains two bidentate 2-oxyiminopropionato anions, which are bonded to the Sn core through the oxime nitrogen atom and one of the carboxylic oxygen atoms forming a *trans* complex with butterfly configuration (Fig. 1a and b). The Sn (II) atom lies on an inversion centre. A distorted trigonal bipyramidal geometry around Sn atom is enforced by the stereochemically active lone pair on tin (II) atom in **1** and **2**, as observed previously[62] and confirmed by τ-test[63]. The Sn–O distances of 2.178(2)-2.204(2) Å in **1**, 2.167(5)-2.175(6) Å in **2** and Sn–N distances 2.508(2)-2.526(2) Å in **1**, 2.487(8)- 2.391(8) Å in **2** are similar to those observed in $Sn_6(O)_4(OSiMe_3)_4$[31], $[^tBuNCONMe_2]_2Sn$[32] as well

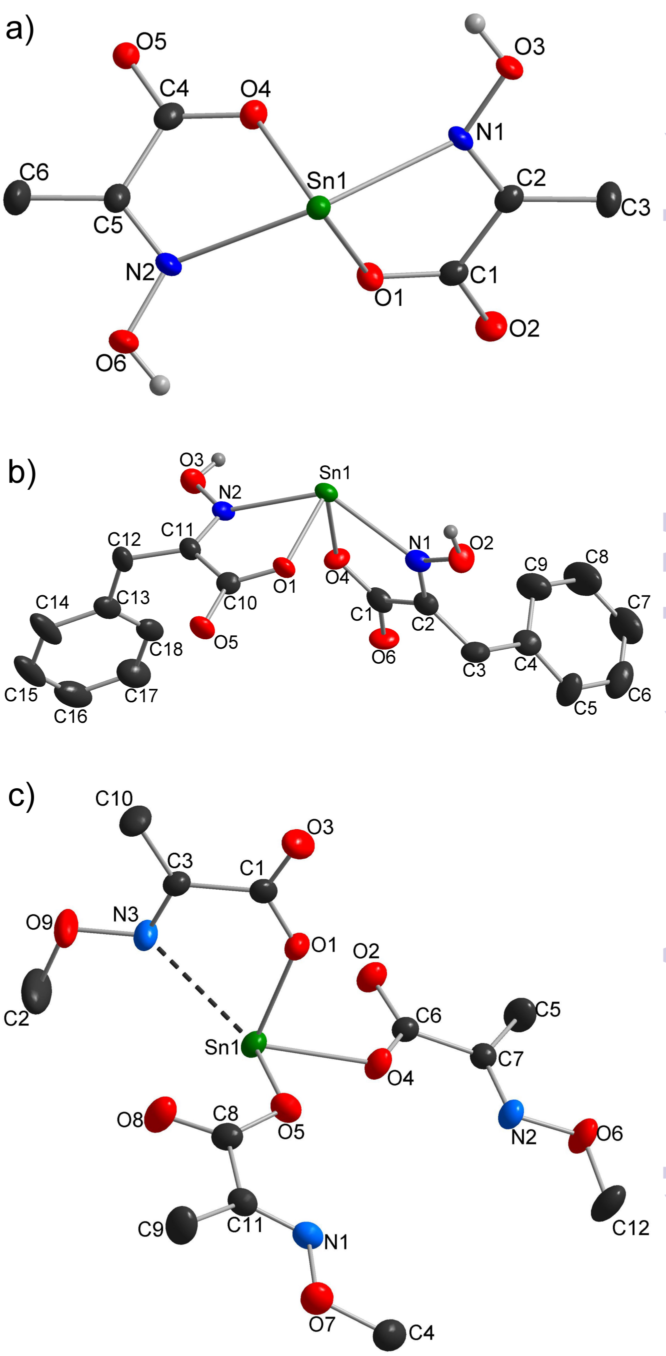

Fig. 1 Solid state structure of a) **1** b) **2** and c) **3**; H atoms on C, and the solvate molecules of **3** were omitted for clarity; thermal ellipsoids are drawn at the 50 % probability level. Selected bond lengths [Å] and angles [deg.]: **1** Sn(1)-O(1) 2.1776(18), Sn(1)-O(4) 2.2038(18), Sn(1)-N(1) 2.508(2), Sn(1)-N(2) 2.526(2), O(1)-Sn(1)-O(4) 85.90(7), O(1)-Sn(1)-N(1) 67.29(7), O(4)-Sn(1)-N(1) 83.38(8), O(1)-Sn(1)-N(2) 83.17(7), O(4)-Sn(1)-N(2) 66.86(8), N(1)-Sn(1)-N(2) 139.50(8), **2** Sn(1)-O(1) 2.167(5), Sn(1)-O(4) 2.175(6), Sn(1)-N(1) 2.487(8), Sn(1)-N(2) 2.391(8), O(4)-Sn(01)-N(1) 67.7(2), O(1)-Sn(1)-O(4) 86.2(3), N(2)-Sn(01)-N(1) 132.9(3), O(1)-Sn(1)-N(2) 70.0(3), O(4)-Sn(1)-N(2) 74.8(2), O(1)-Sn(1)-N(1) 79.9(3), **3** Sn(1)-O(5) 2.1782(12), Sn(1)-O(1) 2.1792(12),Sn(1)-O(4) 2.1988(12), O(5)-Sn(1)-O(1) 82.45(4), O(5)-Sn(1)-O(4) 77.36(4), O(1)-Sn(1)-O(4) 81.55(4), C(1)-O(1)-Sn(1) 133.15(9), C(6)-O(4)-Sn(1)113.13(8), C(8)-O(5)-Sn(1) 112.68(10).

as Sn (II) complexes containing poly-functional ligands.[64-66] The extensive donor type intermolecular hydrogen bonding exists between –NOH and COO groups in both the molecules.

Table 1. Details of the X-Ray data collection and refinement for **1**, **2** and **3**.

Compound	$C_{12}H_{16}N_4O_{12}Sn_2$	$C_{18}H_{16}N_2O_6Sn$	$C_{12}H_{26}N_4O_{11}Sn$
Formula weight	645.68	932.90	521.06
Crystal system	Triclinic	Orthorhombic	Monoclinic
Space group	P-1	$P\,2_12_12_1$	$C\,2/c$
Formula unit, Z	2	4	8
Radiation, λ/ Å		Mo Kα, 0.71073	
Monochromator		Graphite	
Temperature/ K		150(2)	
a/Å	9.3126(6)	12.039(5)	17.653(4)
b/Å	11.0220(6)	12.259(5)	14.077(3)
c/Å	11.5938(6)	12.506(5)	18.854(4)
α/°	113.644(4)	90	90
β/ °	108.010(4)	90	117.11(3)
γ/°	93.80	90	90
V/Å^3	1011.7(4)	1845.7(13)	4170.6(18)
$\rho_{calc.}$/g·cm^{-3}	2.120	1.709	1.660
μ/mm^{-1}	2.538	1.422	1.285
F(000)	624	944	2112
2θ max./°	59.32	58.54	58.44
No. Ref., I>2σ(I)	9854	17869	10110
hkl range	$-12 < h < 12$ $-15 < k < 15$ $-15 < l < 13$	$-16 < h < 16$ $-14 < k < 16$ $-17 < l < 17$	$-24 < h < 22$ $-16 < k < 19$ $-25 < l < 23$
Unique ref., Parameters	5018, 281	4985, 241	5478, 349
R_{int}	0.018	0.129	0.064
$R1^a$	0.020	0.054	0.047
$wR2^b$	0.054	0.075	0.118
GooF^c	1.089	1.072	0.999
Max. / min. Δρ / e·Å^{-3}	0.67/-0.52	0.70/-0.75	0.69/-0.71

[a] $R1 = \Sigma||F_o|-|F_c|| / \Sigma|F_o|$,

[b] $wR2 = \{\Sigma[w(|F_o|^2 - |F_c|^2)^2] / \Sigma[w(|F_o|^4)]\}^{1/2}$ and $w = 1/[\sigma^2(F_o^2)+(nP)^2+mP]$ where $P = (F_o^2+2F_c^2)/3$

[c] $\text{GooF} = [\Sigma_{hkl}w(|F_o|-|F_c|)^2/(n_{data}-n_{var})]^{1/2}$

Short C–O bonding distances of d(C1-O1) = 1.272(3) Å and d(C1-O2) = 1.240(3) Å (**1**) and d(C1-O4) = 1.2774(4) Å and d(C1-O6) = 1.2379(5) Å (**2**) in carboxylic groups suggests π-delocalization, which is probably caused by H-bonding and intermolecular Sn←O dative interactions. Similar π-delocalization of C–O bond is also observed in Co (III), Ni (II) and Zn (II) 2-oxyiminopropionate complexes.[48, 51, 53] The atomic coordinates, anisotropic atomic displacement parameters, bond lengths and angles are listed in table S1-S8 (ESI) respectively.

The first structural difference between **1**, **2** and the previously reported Ni (II), Co (III), Zn (II), Cu (II) and Cd (II) complexes is the long Sn-N bond distance. This bond length ranges between 2.391(2)-2.526(8) Å for **1**, **2** while it is 2.111(1), 1.875(1), 2.334(2), 2.049(2), 2.461(15) Å for Ni-N, Co-N, Zn-N, Cu-N, Cd-N respectively.[48, 51, 53] The long metal-N bond distance is also observed in sodium oximate complex as well.[54] The other interatomic distance in both **1** and **2** are in same range as found in the literature.[45, 67, 68] The second difference is the O-Sn-N bite angle of the ligand to the metal ion. The bite angles in **1** are 67.29°(7), 66.86°(8) and are 70.0°(8) 67.7°(2) in **2**. In the similar Cu(II)[49] complex it is 80.69(6)° and it decreases in Zn(II)[53] 77.69(1)° and Cd(II)[50] 67.88(5)° and 65.77(5)°. The smaller bite angle of the ligand in **1** and **2** as well as in Cd (II) complex is related to the larger ionic radii of Sn (II) and Cd (II) ions.

The Sn atom, in the crystal structure of **3**, is coordinated by three monodentate 2-methoxyiminopropionato- ligands forming perfect trigonal pyramidal geometry with the τ-value of unity[63, 69]. The three-fold coordination of the Sn (II) ion by COO^- groups results in the accumulation of negative charge on Sn atom, which is balanced by NH_4^+ counter ion. The H_2O molecules form H-bonding with oxygen atoms of the carboxyl groups (ESI Fig. S2). The Sn-O distances d(2.178(2) - 2.199(1)Å) are in good agreement with the distances reported in the literature.[69] Similar to **1**, **2** short C-O distances, d(C3-O5) = 1.237(6)Å and d(C3-O4) = 1.287(6)Å, are found in carboxylic group of the 2-methoxyiminopropionato- ligands. However, Sn1…N3 distance is 2.862(1)Å, longest among reported oximato- complex. The atomic coordinates, interatomic distances and angles are listed in table S9-S12 (ESI). The interatomic distances in this structure are close to the distances found in similar tin coordination complexes and tin oxides.[45 67, 68]

Thermal decomposition of 1, 2 and 3

Thermal behaviour of **1-3** were studied under nitrogen and air atmosphere by thermogravimetry, TG coupled IR and mass spectrometry. Fig. 2a is the TG curve for **1** under N_2. The decomposition is not affected by the reaction atmosphere (air or nitrogen) and takes place between 155 – 160 °C. The residual mass observed in N_2 (36.9%) and air (43.4%) agrees well with the theoretical value for the formation of SnO (41.5%) for **1** implying complete decomposition of the ligand. This is supported by the Gram-Schmid curve showing one maximum for the IR signal, indicating simultaneous removal of all

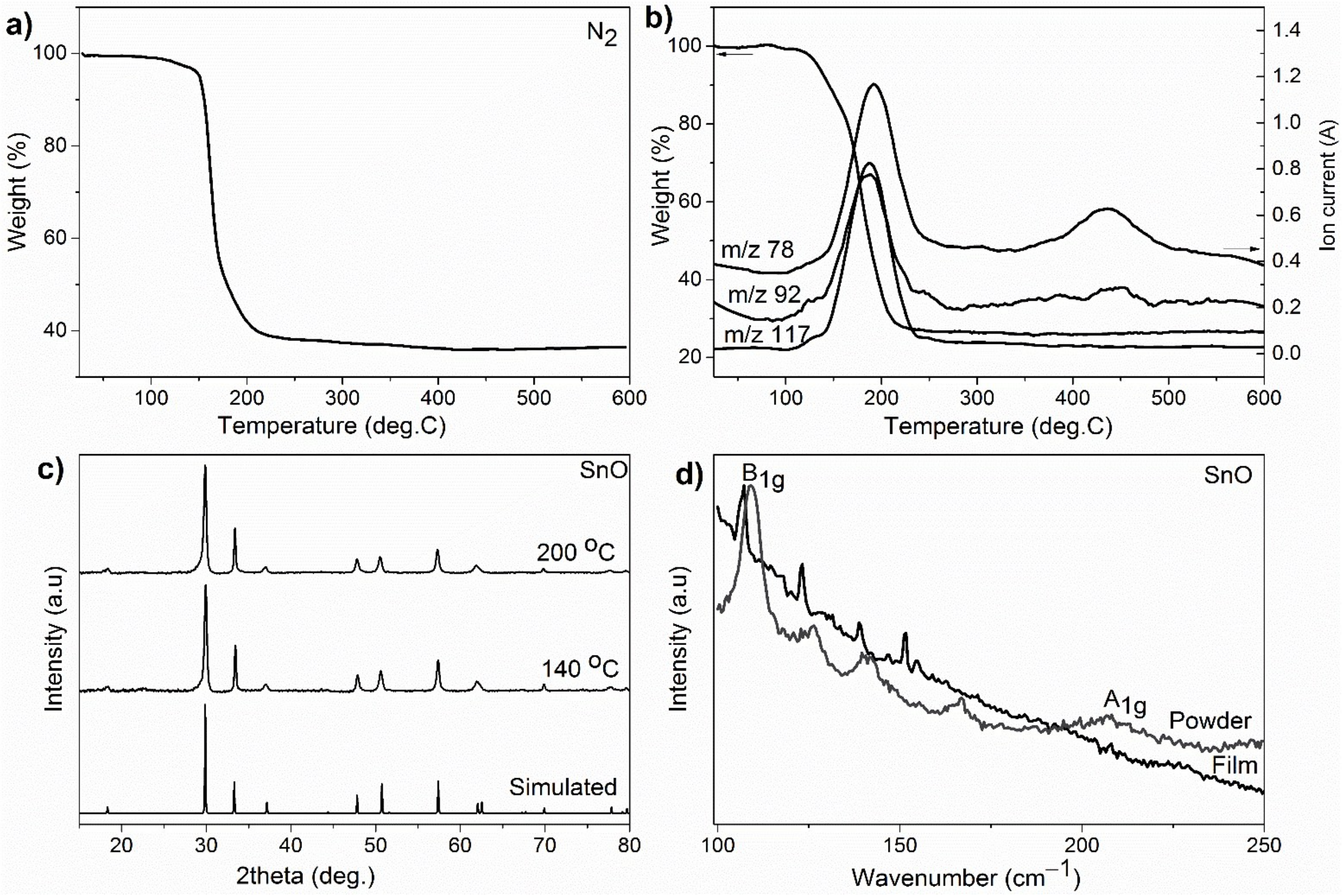

Fig. 2 a) The TG for decomposition of *bis*(2-(hydroxyimino)propionato) tin (II) **1** measured by heating at 10 °C/min. in nitrogen flow of 20 mL/min. b) TG and TG-MS of *bis*[2-(hydroxyimino) 3-phenyl-propionato] tin (II) **2** measured by heating at 5 °C/min. in helium flow of 20 mL/min. The ion current signals are smoothened and normalized. c) XRD and d) Raman spectra of SnO powder and film formed by the decomposition of *bis*(2-(hydroxyimino)propionato) tin (II) **1** at 200 °C.

gaseous fragments (ESI Fig.S3). The IR spectra and mass spectrometry of the gases evolved during the decomposition of **1** could be assigned to water, CO, CO_2, and acetonitrile (ESI Fig. S4 and S5). The fragments observed in the TG-MS of **2** are H_2O, CO, CH_3CN, CO_2 benzene, toluene and benzyl cyanide (Fig. 2b: fragments with higher m/z are only shown). Decomposition of similar Zn and alkali metal complexes indicate a second order Beckmann rearrangement with elimination of CH_3CN, H_2O and CO_2. The metal complex with monoalkylcarbonate ligand is suggested as intermediate, which finally forms the metal oxide.[41, 54] Similar decomposition pathway could be responsible for formation of SnO from **1** and **2** (Scheme 2).

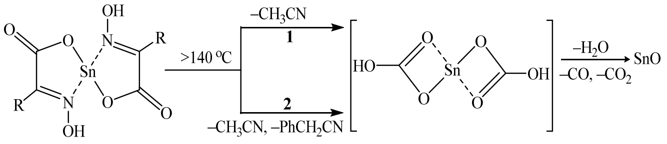

Scheme 2. Proposed decomposition of **1** and **2** based on TG-IR and TG-MS measurements.

The CHN analysis of the residue obtained after heating of **1** in air shows average carbon of 1.65% for decomposition temperature between 140-180 °C, whereas carbon value of 0.86% for temperature of 200 °C (ESI, table 13). Carbon content of <1% has been reported for ZnO films from similar Zn oximate complex at 150 °C and those have been used for FET devices[70]. The decomposition of **2** and **3** in nitrogen follows the same trend as that of complex **1** (ESI Fig. S6). In air **2** and **3** undergo additional weight loss at higher temperature, attributed to the removal of surface organic carbon.

Tin (II) oxide synthesis

SnO was synthesized by decomposing **1** and **2**, whereas **3** has not been used for the decomposition study due to its low yield during synthesis.

SnO powder formation from **1** *and* **2**

1 and **2** are heated from 140-200 °C for one hour in air. SnO formation is observed at 140 °C itself for **1** (Fig. 2c). The crystallinity of the formed SnO independent of decomposition

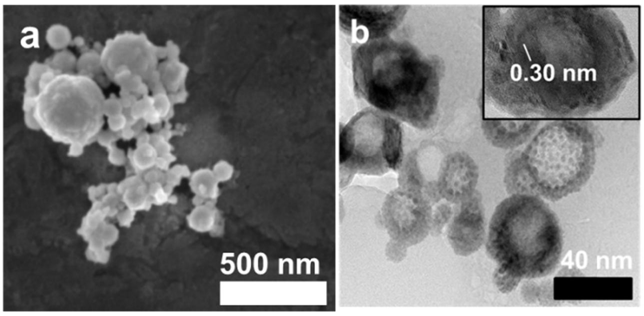

Fig. 3 a) SEM b) TEM images of SnO from the decomposition of **1** at 200 °C. Spherical particles observed at 200 °C and composed of smaller particles of 10 nm grouped together as well as forming hollow spheres. Inset: Atomic fringes of 101 plane of SnO.

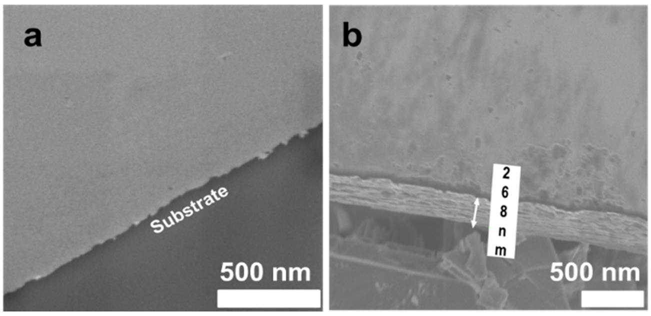

Fig. 4 SEM micrograph of SnO film a) after one layer b) after 16 layers, formed by spin-coating and decomposing of **1** at 200 °C.

temperature (140-200 °C). Amorphous SnO was obtained from **2** even at 200 °C (ESI Fig. S7). The formation of amorphous SnO from **2** could be attributed to incomplete removal of the benzene fragment during the decomposition at 163 °C. This is supported by the appearance of signal for benzene (m/z 78) and toluene (m/z 92) fragment at above 400 °C during the decomposition of **2** (Fig. 2b). Hence, **1** was chosen for making nanoparticle and thin films of SnO. The average crystallite size of SnO from **1** is in the range of 47-50 nm for temperatures between 140-200°C, determined by Scherrer equation. Raman spectra of SnO from **1** recorded from 100-500 cm^{-1} show two vibrational absorptions at 109 and 209 cm^{-1} corresponding to characteristic B_{1g} and A_{1g} modes of SnO[32] (Fig. 2d). The similarity of the Raman spectra for both 140 °C and 200 °C shows similar decomposition at these temperatures (ESI Fig.S8).

Scanning and transmission electron microscope images of SnO particle formed at 200°C is shown in Fig. 3a and b respectively. At 200°C SnO particles appear spherical in shape and have rough surface morphology. The particle size is between 50-250 nm. At 140°C they are lumped together, with fewer non-agglomerated particles. The particle size is between 100-150 nm at 140°C (ESI Fig. S9). Transmission electron microscope images (Fig. 3b) of the SnO particles at 200 °C indicate the presence of hollow and dense SnO particles. The high resolution TEM image (inset: Fig. 3b) show lattice fringes of 0.30 nm spacing corresponding to (101) plane of SnO.

Comparison with spherical SnO particles from **1** with those prepared by aqueous route using $Sn_6O_4(OH)_4$ derived from tin halides and amides[9, 11, 71] or by vapour deposition and carbothermal reaction of SnO[8, 12] reveal various hierarchical morphologies such as nanoribbons, nanobelts, dendrimers and meshes. In addition, some level of control on oxidation state in the final tin oxide has been achieved through the use of well-defined Sn (II) centred precursors. However, rapid precipitation in aqueous route and formation of sub-stoichiometric tin oxide in vapour based methods are not suitable for thin film preparation. The tin oximate thus provides process flexibility for thin film preparation.

SnO thin film from 1

Thin films of SnO are prepared by spin-coating a saturated solution of **1** in methanol or ethylene glycol/methanol mixture (1:9 v/v). The SEM micrograph of the single and 16 layers of SnO film on Si substrate, from ethylene glycol/methanol mixture, after heating the substrate to 200 °C is shown in Fig. 4a and b respectively. The energy-dispersive X-ray spectroscopy (EDX) analysis confirmed the presence of tin in the film for single layer SnO deposition (ESI Fig. S10). The 16 layer spin coated sample show a film thickness of 268 nm. Thus, the average thickness per layer is estimated to be 16-20 nm on silicon substrate. Comparing the morphology of SnO thin films from reported metalorganic precursors[31, 32, 34] showed platelets and cubes with several grain boundaries, whereas with **1** smooth films could be obtained over larger area.

UV-Vis spectra of the SnO film measured in the diffuse reflection setup shows a band gap in the range of 3.0-3.3 eV (ESI Fig. S11) and is comparable to the reported data[72]. X-ray photoelectron spectroscopy (XPS) for sample spin coated to 10 layers of SnO is shown in Fig. S12a-c (ESI). XPS survey spectrum of the SnO layer indicates incorporation of carbon and small amount of nitrogen (ESI, Fig. S13 and S14). The occlusion of these elements could be due to the residual solvent remaining or incomplete removal of the decomposition product of **1** during several heating cycle. The binding energies at 487.0 and 495.4 eV can be assigned to Sn 3d$_{5/2}$ and 3d$_{3/2}$ electrons of tin[28] (Fig. S12a, ESI). The O1s spectral line shows binding energies at 530.8 eV and 532.4 eV. The binding energy of 530.8 can be correlated to lattice oxygen in the tin oxide film and 532.4 for adsorbed OH on the surface [73] (Fig. S12b, ESI). The valence band spectral peaks at 9 eV and below 2 eV[32, 74] due the formation of antibonding and bonding Sn(II) 5s-O2p states were not observed, indicating surface of the SnO film from **1** has oxidised to Sn(IV) (Fig. S12c ESI). Thus it can be concluded that the SnO film reacts with adsorbed/atmospheric oxygen to convert to SnO$_2$ as observed in the XPS analysis. Similar surface oxidation was observed for SnO film deposited from Sn(II) bis(ureide) during its exposure to ambient atmosphere.[32]

To understand the oxidation of deposited SnO thin film, a drop-cast film from **1** in DMF solution on Si substrate is analysed by IR before heating and by Raman spectroscopy after heating to 200°C. IR of the precursor film on Si and **1** as powder show same absorption bands (ESI, Fig. S15) indicating that **1** remain in Sn (II) state on the substrate. Raman spectra of the SnO film formed after heating to 200°C shows both the characteristic B_{1g} and A_{1g} vibrational modes (Fig. 2d) in agreement with the SnO powder produced from **1** at 200°C. This result clearly indicates the observed Sn (IV) state in the XPS analysis is due to the surface oxidation.

The SnO thin films formed from the reported metalorganic precursor e.g. $Sn_6O_4(OSiMe_3)_4$, $[\{Sn(OSiMe_3)_2\}_2]$, Sn(II)*bis*(ureide) (ureide = $^tBuNCONMe_2$), $[Sn(\mu\text{-}ONep)_2]_\infty$ (ONep = OCH_2CMe_3)[31] [32] [34] indicate stringent control of oxygen environment, higher deposition temperature (> 300°C) and formation of metallic Sn along with the desired tin (II) oxide phase. The air/moisture sensitivity of these precursors and the disproportionation of SnO to Sn and SnO_2 at higher temperature make the process complicated. The air/moisture stability, low decomposition temperature and solubility of **1** in common organic solvent makes it suitable for large area processing such as spin coating and printing.

Thin films of SnO of thickness 30 - 50 nm and 300 – 400 nm were prepared on the interdigitated substrate at 200 °C. The I-V characteristics of these films in the forward bias indicate the semiconducting property of the film (ESI Fig. S16 and S17) with a breakdown voltage at 8.9 V in the forward bias. Further studies to understand the thin film behaviour for transistor application is currently underway.

Conclusions

Tin (II) ketoacidoximate complexes were successfully synthesized and characterized. The Sn atom is four-fold coordinated and is donor stabilised by the oxime nitrogen of the ligand in all the complexes. The *bis*[2-(hydroxyimino) propionato] tin (II) decompose above 140 °C both in air and nitrogen with complete elimination of ligand to form SnO. The SnO particles of average size 50 nm were synthesized below 200°C by heating **1**. SnO thin films of 16-20 nm thickness were prepared by spin-coating. The films slowly convert to Sn (IV) oxide at the surface on exposure to air. The bulk of the film remain in Sn(II) state. The ambient atmosphere synthesis and processing makes Sn(II) oximate attractive for solution processable application.

Experimental section

Reagents and General Procedures

All the syntheses were performed in ambient atmosphere and with deionized water. $SnCl_2{\cdot}2H_2O$ (98%, Alfa Aesar), pyruvic acid (98%, Alfa Aesar), sodium phenyl pyruvate (98%, Sigma-Aldrich), hydroxylamine hydrochloride (99%, Sigma-Aldrich), methoxylamine hydrochloride (98%, Sigma-Aldrich), ammonium bicarbonate (≥ 99%, Sigma-Aldrich), methanol, ethanol and N,N-dimethylformamide HPLC grade are used as-received. The melting point/decomposition of **1-3** were determined from the DTA (ESI Fig. S18)

Precursor synthesis

Syntheses of Sn ketoacidoximato complexes were an adaptation of method described previously.[53, 57, 60] The *in-situ* generation of the α-ketoacid oxime ligand in water was carried out according to the procedure described by Spenser *et al.*[40]

Synthesis of *bis*[2-(hydroxyimino) propionato] tin (II) (**1**)

Ammonium bicarbonate (9.49 g, 120 mmol) was added portion wise to a stirred solution of hydroxylamine hydrochloride (4.17 g, 60 mmol) and pyruvic acid (5.28 g, 60 mmol) in water (50 mL) at room temperature and the mixture was stirred until all gas evolution had ceased. $SnCl_2{\cdot}2H_2O$ (6.77 g, 30 mmol) was then added, and the mixture was stirred for 4 h, after which a white powder of **1** was filtered off and washed with ice cold water. The single crystals were obtained from concentrated ethanol solution of the compound at -35°C, Yield (6.5 g, 67%), mp 161°C (TG) (decomp.), Found: C, 22.3; H, 2.5; N, 8.6, Calc. for $C_6H_8N_2O_6Sn$: C, 22.3; H, 2.5; N, 8.7%, IR (ν_{max}/cm^{-1}) ATR, powder: 3170 (w), 3050 (w), 2797 (w), 2725 (w), 1584 (s), 1487 (ms), 1366 (s), 1345 (s), 1195 (s), 1049 (s), 851(s), 759 (ms), 732 (s). ^{1}H NMR (400 MHz;$(CD_3)_2SO$, 25 °C), δ: 1.95 (s, 6H, CH_3-C=N); ^{13}C NMR (100 MHz; $(CD_3)_2SO$, 25 °C) δ: 11.5 (CH$_3$-C=N), 151.1 (C=N), 167.2 (C=O).

Synthesis of *bis*[2-(hydroxyimino)3-phenyl-propionato] tin (II) (**2**)

Ammonium bicarbonate (0.395 g, 5 mmol) was added portion wise to a solution of hydroxylamine hydrochloride (0.347 g, 5 mmol) in 10 mL water and the mixture was stirred until all gas evolution had ceased. To the above solution sodium phenyl pyruvate (0.931g, 5mmol) in water (10 mL) was added at room temperature. The reaction was allowed to continue for 2 h. To the above mixture $SnCl_2{\cdot}2H_2O$ (0.564 g, 2.5 mmol) was then added, and the mixture was stirred for 4 h, after which a creamy yellow powder **2** was filtered off and washed with ice cold water. The single crystals were obtained from concentrated methanol solution by slow evaporation method. Yield (1 g, 78%) mp 163°C (TG) (decomp.) Found C, 44.1; H, 3.4; N, 6.1, Calc. for $C_{18}H_{16}N_2O_6Sn$: C, 45.5; H, 3.4; N, 5.9%, IR (ν_{max}/cm^{-1}), ATR, powder: 3175 (w), 3062 (w), 2846 (w), 1600 (s), 1493 (m), 1453 (w), 1426 (w), 1373 (ms), 1337 (w), 1298 (w), 1230 (ms), 1158 (ms), 1137 (ms), 1055 (s), 1026 (s), 931 (w), 862 (s), 774 (ms), 754 (m), 715 (s), 695 (s), 552 (w). ^{1}H NMR (400 MHz; $(CD_3)_2SO$, 25 °C), δ: 3.83 (s, 4H, -CH_2-Ph), 7.24 (s, 10H, Ph) 12.4 (s, 2H,-N-OH); ^{13}C NMR (100 MHz; $(CD_3)_2SO$, 25 °C) δ: 30.7(−CH$_2$), 126.6 (Ph), 128.7 (Ph), 129.2 (Ph), 137.1(Ph) 152.2 (C=N), 167.1 (C=O).

Synthesis of Diaqua *tris*[2-(methoxyimino) propionato] tin(II) ammonium salt (**3**)

Ammonium bicarbonate (9.49 g, 120 mmol) was added portionwise to a stirred solution of methoxylamine hydrochloride (5.01 g, 60 mmol) and pyruvic acid (5.28 g, 60 mmol) in water (30 mL) at room temperature, and the mixture was stirred until all gas evolution had ceased and stirred further for 3h. $SnCl_2 \cdot 2H_2O$ (6.77 g, 30 mmol) was then added; at the start reaction is slow. As the time progresses a white precipitate is seen. The precipitate is dissolved in ethanol, reduced in volume and kept at -35°C for recrystallization. Yield (0.8 g, 10%) mp 151°C (TG) (decomp.) Found C: 27.9, H: 4.2, N: 10.3, Calc. for $C_{12}H_{26}N_4O_{11}Sn$: Calc. C: 27.7, H: 5.0, N: 10.8%. IR (ν_{max}/cm^{-1}), ATR, powder: 3284 (w), 3144 (w), 3052 (w), 2988 (w), 2943 (w), 2827 (w) 1649 (ms),1633 (s), 1593(s), 1536 (m), 1442 (m), 1418 (ms), 1371 (w), 1349 (s), 1204(s), 1172 (s), 1043, (s) 927 (ms), 855 (s), 768 (m), 723 (s), 579(m); ^{1}H NMR (400 MHz; $(CD_3)_2SO$, 25 °C), δ: 1.91 (s, 9H, N=C-CH_3), 3.93 (s, 9H, N-OCH_3); ^{13}C NMR (100 MHz; $(CD_3)_2SO$, 25 °C) δ: 12.3(N=C-CH$_3$), 62.4(N-OCH$_3$), 152.7 (C=N), 168.0 (C=O).

Synthesis of SnO

*Heating **1***

150 mg of the complex **1** is heated in a nickel crucible to 140 – 200°C in air for one hour in a general purpose laboratory furnace. 52 mg (yield 100% based on Sn content)

Thin film deposition-spin coating

Saturated solution of **1** in methanol or ethylene glycol mixture (9:1) is used to spin-coat a thin layer of precursor on Si substrate. A filtered, 50 μL of the solution is dropped on the substrate with coating programme 1000 rpm/30 seconds/5000 rpm/20 seconds. The relative humidity during spin coating was between 57-60 %.

Thin film deposition-drop casting

100 μL of saturated solution of **1** in DMF is drop-cast on Si substrate. The solvent is allowed to evaporate in a well-ventilated chemical hood.

Characterization

IR spectroscopic measurements were carried out using Nicolet iS10 FTIR spectrometer with ATR setup. The scans were performed from 4000 – 525 cm^{-1}. ^{1}H NMR and ^{13}C NMR spectra were recorded on a Bruker AC300F spectrometer at 400 MHz. Elemental analysis (C,H,N) was performed in Flash 2000 instrument from thermo scientific. Thermogravimetry measurements were carried out using a Netzsch STA 449 F3 Jupiter instrument equipped with a TG/DSC sample carrier. Thermogravimetry coupled infra-red (TG-IR) measurements were performed on a Netzsch TGA 289 F1 Iris instrument coupled to a Tensor 27 TGA-IR. Thermogravimetry coupled mass spectrometry (TG-MS) measurements were carried out on a Netzsch TG 209 F1 Iris coupled with QMS 403 C Aelos mass spectrometer. Micro Raman measurements were performed on LabRAM HR high resolution microscope from Horiba Jobin Yvon model HR 800. The excitation wavelength was 532.2 nm. The spectrum was recorded in the range of 50 – 1000 cm^{-1}. X-ray powder diffraction patterns (XRD) of the samples at room temperature were recorded using a STOE Stadi MP instrument equipped with Cu-Kα_1 source and Mythen detector. SEM investigations were performed with Quanta 600 FEG microscope typically at low keV (3 – 5 keV). TEM analysis was conducted on a Titan Super Twin instrument at 300 kV.
Single-crystal X-ray diffraction experiments for **1**–**3** were carried out on IPDS2 (STOE) image plate diffractometer with graphite monochromatized Mo-$K\alpha$ (λ = 0.71069 Å) radiation, at 150 K with a detector distance of 100 mm. Single crystals of **1-3** were mounted on a glass capillary using perfluoroalkylether (viscosity 1800cSt., ABCR GmbH & Co. KG Karlsruhe. For data collection, determination, and refinement of the lattice parameters as well as for data reduction including LP correction, the STOE X-Area[75] software package was used. The intensity data were corrected for absorption numerically using the crystal habit and the program X-Shape.[76] The crystal structure was solved by direct methods and refined using the program packages SHELXS97 and SHELXL97.[77]

Acknowledgements

This work was supported by the King Abdullah University of Science & Technology (KAUST) baseline (BAS/1/1302-01-01) and AEA funding. J. K. thanks, Dr. Rachid Sougrat and Ms. Nini Wei for TEM imaging, Dr. Mohamed Nejib Hedhili for XPS analysis.

Notes and references

[a] Physical Sciences and Engineering Division, 4700 King Abdullah University of Science & Technology (KAUST), Thuwal, 23955-6900, Kingdom of Saudi Arabia.
* to whom correspondence should be made
e-mail: alexander.rothenberger@kaust.edu.sa
Fax: +966 12 8021258, Phone: +966 12 808 0745

†Electronic Supplementary Information (ESI) available: [IR, gas phase IR, mass of decomposition products, UV-Vis spectrum of SnO thin film. Details on data collections, refinements, atomic coordinates, anisotropic atomic displacement parameters, bond lengths and angles for the reported complexes, XRD and SEM of decomposition product of **2**, XPS, I-V characteristics of the film]. See DOI: 10.1039/b000000x/

References

1. P. P. Edwards, A. Porch, M. O. Jones, D. V. Morgan and R. M. Perks, *Dalton Trans.*, 2004, 2995-3002.
2. B. G. Lewis and D. C. Paine, *MRS Bull.*, 2000, **25**, 22-27.
3. E. N. Dattoli, Q. Wan, W. Guo, Y. Chen, X. Pan and W. Lu, *Nano Lett.*, 2007, **7**, 2463-2469.
4. C. W. Ou, Dhananjay, Z. Y. Ho, Y. C. Chuang, S. S. Cheng, M. C. Wu, K. C. Ho and C. W. Chu, *Appl. Phys. Lett.*, 2008, **92**, 122113.
5. M. Batzill and U. Diebold, *Prog. Surf. Sci.*, 2005, **79**, 47.

6. J. R. Brown, M. T. Cheney, P. W. Haycock, D. J. Houlton, A. C. Jones and E. W. Williams, *J. Electrochem. Soc.*, 1997, **144**, 295-299.
7. G. Frank, E. Kauer, H. Köstlin and F. J. Schmitte, *Sol. Energ. Mater.*, 1983, **8**, 387-398.
8. B. Kumar, D. H. Lee, S. H. Kim, B. Yang, S. Maeng and S.-W. Kim, *J. Phys. Chem. C*, 2010, **114**, 11050-11055.
9. H. Uchiyama and H. Imai, *Langmuir*, 2008, **24**, 9038-9042.
10. Z. L. Wang and Z. W. Pan, *Adv. Mater.*, 2002, **14**, 1029-1032.
11. H. Uchiyama and H. Imai, *Cryst. Growth Des.*, 2007, **7**, 841-843.
12. M. O. Orlandi, E. R. Leite, R. Aguiar, J. Bettini and E. Longo, *J. Phys. Chem. B*, 2006, **110**, 6621-6625.
13. D. Aurbach, A. Nimberger, B. Markovsky, E. Levi, E. Sominski and A. Gedanken, *Chem. Mater.*, 2002, **14**, 4155-4163.
14. N. Xiao, C. Li, D. Li, B. Liu, B. Zou, G. Zou, W. W. Yu, J. Ning, Q. Dai, T. Jiang, K. Men and D. Liu, *Langmuir*, 2009, **25**, 1818-1821.
15. H. Giefersa, F. Porschb and G. Wortmanna, *Solid State Ionics*, 2005, **176**, 199-207.
16. Y. He, D. Li, J. Chen, Y. Shao, J. Xian, X. Zheng and P. Wang, *RSC Adv.*, 2014, **4**, 1266-1269.
17. Z. R. Dai, Z. W. Pan and Z. L. Wang, *J. Am. Chem. Soc.*, 2002, **124**, 8673-8680.
18. H. Wang, Y. Wang, J. Xu, H. Yang, C.-S. Lee and A. L. Rogach, *Langmuir*, 2012, **28**, 10597-10601.
19. Y. Ogo, H. Hiramatsu, K. Nomura, H. Yanagi, T. Kamiya, M. Hirano and H. Hosono, *Appl. Phys. Lett.*, 2008, **93**, 032113.
20. H. Hosono, Y. Ogo, H. Yanagi and T. Kamiya, *Electrochem. Solid-State Lett.*, 2011, **14**, H13-H16.
21. K. Nomura, T. Kamiya and H. Hosono, *Adv. Mater.*, 2011, **23**, 3431-3434.
22. J. Um and S. E. Kim, *ECS Solid State Lett.*, 2014, **3**, P94-P98.
23. L. Liang and H. Cao, *ECS Trans.*, 2013, **50**, 289-297.
24. I. C. Chiu and I. C. Cheng, *IEEE Electron Device Lett.*, 2014, **35**, 90-92.
25. P.-C. Hsu, W.-C. Chen, Y.-T. Tsai, Y.-C. Kung, C.-H. Chang, C.-J. Hsu, C.-C. Wu and H.-H. Hsieh, *Jpn. J. Appl. Phys.*, 2013, **52**, 05DC07-05DC07-06.
26. L. Y. Liang, Z. M. Liu, H. T. Cao, W. Y. Xu, X. L. Sun, H. Luo and K. Cang, *J. Phys. D*, 2012, **45**, 085101.
27. H. Yabuta, N. Kaji, R. Hayashi, H. Kumomi, K. Nomura, T. Kamiya, M. Hirano and H. Hosono, *Appl. Phys. Lett.*, 2010, **97**, 072111.
28. A. C. Saritha, K. S. Sasanka, M. Majeesh, K. Hasna, P. P. Subha, L. S. Vikas and M. K. Jayaraj, *J. Electr. Devices*, 2014, **19**, 1642 - 1647.
29. H. Luo, L. Y. Liang, H. T. Cao, Z. M. Liu and F. Zhuge, *ACS Appl. Mater. Interfaces*, 2012, **4**, 5673-5677.
30. T. Toyama, Y. Seo, T. Konishi, H. Okamoto and Y. Tsutsumi, *Appl. Phys. Express*, 2011, **4**, 071101.
31. I. Barbul, A. L. Johnson, G. Kociok-Köhn, K. C. Molloy, C. Silvestru and A. L. Sudlow, *ChemPlusChem*, 2013, **78**, 866-874.
32. T. Wildsmith, M. S. Hill, A. L. Johnson, A. J. Kingsley and K. C. Molloy, *Chem. Commun.*, 2013, **49**, 8773-8775.
33. J. H. Han, Y. J. Chung, B. K. Park, S. K. Kim, H.-S. Kim, C. G. Kim and T.-M. Chung, *Chem. Mater.*, 2014, **26**, 6088-6091.
34. T. J. Boyle, T. L. Ward, S. M. De'Angeli, H. Xu and W. F. Hammetter, *Chem. Mater.*, 2003, **15**, 765-775.
35. K. Okamura, B. Nasr, R. A. Brand and H. Hahn, *J. Mater. Chem.*, 2012, **22**, 4607-4610.
36. X. Q. Pan and L. Fu, *J. Appl. Phys.*, 2001, **89**, 6048-6055.
37. W. K. Choi, H. Sung, K. H. Kim, J. S. Cho, S. C. Choi, H. J. Jung, S. K. Koh, C. M. Lee and K. Jeong, *J. Mater. Sci. Lett.*, 1997, **16**, 1551 - 1554.
38. V. Y. Kukushkin and A. J. L. Pombeiro, *Coord. Chem. Rev.*, 1999, **181**, 147-175.
39. N. Gerasimchuk, *Eur. J. Inorg. Chem.*, 2014, DOI: 10.1002/ejic.201402251, 4518–4531.
40. A. Ahmad and I. D. Spencer, *Can. J. Chem.*, 1961, **39**, 1340-1359.
41. J. J. Schneider, R. C. Hoffmann, J. Engstler, S. Dilfer, A. Klyszcz, E. Erdem, P. Jakes and R. A. Eichel, *J. Mater. Chem.*, 2009, **19**, 1449-1457.
42. N. Gerasimchuk, T. Maher, P. Durham, K. V. Domasevitch, J. Wilking and A. Mokhir, *Inorg. Chem.*, 2007, **46**, 7268−7284.
43. A. Szorcsik, L. Nagy, L. Pellerito and R. D. Lampeka, *J. Radioanal. Nucl. Chem.*, 2003, **257**, 285-291.
44. R. Lampeka, R. Bergs, R. Krämer, K. Polborn and K. Beck, *Z. Naturforsch. B*, 1994, **49**, 225 - 232.
45. R. Krämer, H. Wanjek, K. Polborn and W. Beck, *Chem. Ber.*, 1993, **126**, 2421-2427.
46. T. Y. Sliva, R. D. Lampeka, G. V. Vladyko, E. I. Boreko and L. V. Korobchenko, *Pharmaceut. Chem. J.*, 1992, **26**, 613-615.
47. A. W. Apblett and G. D. Georgieva, *Phosphorus, Sulfur Silicon Relat. Elem.*, 2009, **93**, 479-480.
48. R. D. Lampeka, N. M. Dudarenko and V. V. Skopenko, *Acta Cryst.*,, 1994, **C50**, 706-708.
49. M. V. Kirillova, M. Haukka, A. M. Kirillov, J. A. L. Silva, J. J. R. Frausto da Silva and A. J. L. Pombeiro, *Acta Crystallogr. Sect. E*, 2007, **63**, m1670-m1671.
50. I. Georgieva, N. Trendafilova and G. Bauer, *Spectrochim. Acta A*, 2006, **63**, 403-415.
51. R. D. Lampeka, Z. D. Uzakbergenova and V. V. Skopenko, *Z. Naturforsch. B*, 1993, **48**, 409-417.
52. A. Kufelnicki, S. V. Tomyn, V. Vitske, J. Jaciubek-Rosińska, M. Haukka and I. O. Fritsky, *Polyhedron*, 2013, **56**, 144-151.
53. M. R. Hill, A. W. Jones, J. J. Russell, N. K. Roberts and R. N. Lamb, *Inorg. Chim. Acta*, 2005, **358**, 201-206.
54. A. W. Apblett, G. D. Georgieva and J. T. Mague, *Inorg. Chem.*, 1997, **36**, 2656-2661.
55. A. W. Apblett, G. D. Georgieva and J. T. Mague, *Can. J. Chem.*, 1997, **75**, 483 - 490.
56. K. Malek, M. Vala, J. Swiatek-Kozlowska and L. M. Proniewicz, *New J. Chem.*, 2004, **28**, 477-483.
57. Z. Zhang, R. Liu, M. Zhao and Y. Qian, *Mater. Chem. Phys.*, 2001, **71**, 161-164.
58. Y. S. Wang, P. J. Thomas and P. O'Brien, *J. Phys. Chem. B*, 2006, **110**, 4099-4104.
59. Y. S. Wang, *J. Cryst. Growth*, 2006, **291**, 398-404.
60. J. Khanderi, C. Contiu, J. Engstler, R. C. Hoffmann, J. J. Schneider, A. Drochner and H. Vogel, *Nanoscale*, 2011, **3**, 1102-1112.
61. M. Pashchanka, R. C. Hoffmann and J. J. Schneider, *J. Mater. Chem.*, 2010, **20**, 957-963.
62. C. Pettinari, F. Marchetti, R. Pettinari, A. Cingolani, E. Rivarola, C. Phillips, J. Tanski, M. Rossi and F. Caruso, *Eur. J. Inorg. Chem.*, 2004, **2004**, 3484-3497.
63. A. W. Addison, T. N. Rao, J. Reedijk, J. van Rijn and G. C. Verschoor, *J. Chem. Soc., Dalton Trans.*, 1984, 1349-1356.
64. L. Iovkova-Berends, T. Berends, T. Zöller, G. Bradtmöller, S. Herres-Pawlis and K. Jurkschat, *Eur. J. Inorg. Chem.*, 2012, **2012**, 3191-3199.
65. L. Iovkova-Berends, T. Berends, T. Zöller, D. Schollmeyer, G. Bradtmöller and K. Jurkschat, *Eur. J. Inorg. Chem.*, 2012, **2012**, 3463-3473.
66. T. Berends, L. Iovkova, G. Bradtmöller, I. Oppel, M. Schürmann and K. Jurkschat, *Z. Anorg. Allg. Chem.*, 2009, **635**, 369-374.
67. L. Gracia, A. Beltrán and J. Andrés, *J. Phys. Chem. B*, 2007, **111**, 6479-6485.
68. D. Le Bellac, J. M. Kiat, P. Garnier, H. Moudden, P. Sciau, P. A. Buffat and G. André, *Phys. Rev. B*, 1995, **52**, 13184-13194.
69. E. Hennings, H. Schmidt, M. Kohler and W. Voigt, *Acta Crystallogr. Sect. E*, 2014, **70**, 474-476.
70. J. J. Schneider, R. C. Hoffmann, J. Engstler, O. Soffke, W. Jaegermann, A. Issanin and A. Klyszcz, *Adv. Mater.*, 2008, **20**, 3383-3387.
71. J. Khanderi, L. Shi and A. Rothenberger, *Inorg. Chim. Acta*, 2015, **427**, 27-32.
72. W. Guo, L. Fu, Y. Zhang, K. Zhang, L. Y. Liang, Z. M. Liu, H. T. Cao and X. Q. Pan, *Appl. Phys. Lett.*, 2010, **96**, 042113.
73. L. Yan Liang, H. Tao Cao, X. Bo Chen, Z. Min Liu, F. Zhuge, H. Luo, J. Li, Y. Cheng Lu and W. Lu, *Appl. Phys. Lett.*, 2012, **100**, 263502.
74. L. Kover, Z. Kovacs, R. Sanjines, G. Moretti, I. Cserny, G. Margaritondo, J. Palinkas and H. Adachi, *Surf. Interf. Anal.*, 1995, **23**, 461 - 466.

75. X-Area, *STOE's Area Detector Software and IPDS software, STOE & Cie., Darmstadt*, 2006.
76. X-Shape, *Crystal Optimisation for Numerical Absorption Correction, STOE & Cie., Darmstadt*, 1999.
77. G. M. Sheldrick, *SHELX97, Programs for the Solution and Refinement of Crystal Structures, University of Goettingen, Germany*, 1997.